Influence of sodium on the potential-induced degradation for n-type crystalline silicon photovoltaic modules

Keisuke Ohdaira[1], Yutaka Komatsu[1], Tomoyasu Suzuki[1], Seira Yamaguchi[1], and Atsushi Masuda[2]

[1]Japan Advanced Institute of Science and Technology, Nomi, Ishikawa 923-1292, Japan

[2]National Institute of Advanced Industrial Science and Technology, Tsukuba, Ibaraki 305-8568, Japan

We precisely investigate sodium (Na)-induced potential-induced degradation (PID) in n-type front-emitter (n-FE) crystalline silicon (c-Si) photovoltaic (PV) modules, in which open-circuit voltage (V_{oc}) and fill factor (FF) deteriorate. Secondary ion mass spectrometry (SIMS) shows Na introduction into n-FE cells by a negative-bias PID stress and a reduction in Na density by positive-bias application. Scanning electron microscopy (SEM) and energy dispersive X-ray (EDX) analysis reveal the formation of Na-based protrusions on the cell surface. Silicon nitride (SiN_x) disappears at the position of protrusions, which is the root cause for the serious and unrecoverable PID of n-FE c-Si PV modules.

Crystalline silicon (c-Si) wafer-based photovoltaic (PV) modules dominate the present PV market, and most of the c-Si cells in the PV modules are p-type wafer-based ones due to their matured fabrication processes.[1)] On the other hand, n-type c-Si wafer-based PV modules will have more PV market in the near future because of their superior performance to p-type ones[2–8)] and higher stability against light soaking due to the absence of the formation of boron-oxygen complexes.[9–11)] When the c-Si PV modules are installed in large-scale PV power plants, their long-term reliability must be ensured. One of the most significant reliability issues of PV modules is potential-induced degradation (PID), performance loss of PV modules triggered by a difference in an electrical potential between a grounded aluminum (Al) frame and cells.[12)] The mechanism of PID for the p-type c-Si wafer-based PV modules has been considerably clarified,[13–16)] and several ways to prevent their PID have also been already proposed.[17–20)] In contrast, the PID of n-type wafer-based c-Si PV modules has not been fully investigated yet.[12, 21–23)]

We have thus far investigated the PID of PV modules with n-type c-Si wafer-based front-emitter (n-FE)[24–26)] and rear-emitter[27)] homojunction cells and Si heterojunction cells.[28,29)] For the PID of n-FE PV modules, we have observed three stage degradations taking place at different PID-stress durations with different behaviors. The first PID, characterized by reductions in short-circuit current density (J_{sc}) and open-circuit voltage (V_{oc}) while keeping fill factor (FF), is due to the accumulation of positive charges in a silicon nitride (SiN_x) passivation film, inducing increased density of minority carries in a p^+ emitter, electrons, near the interface which causes more active surface recombination, as also demonstrated earlier.[21,22)] We have clarified that K^+ centers in the SiN_x are the most likely candidate for the origin of the positive charges.[24,25)] The second PID, characterized by a reduction in FF alone not due to a decrease in shunt resistance but due

to an increase in a diode ideality factor, is probably induced by the introduction of impurity atoms, such as sodium (Na), into a depletion region.[26] The third PID, characterized by further reductions in V_{oc} and FF, may be related to more serious introduction of Na into n-FE cells. We, however, have not obtained the actual evidence for the influence of Na on the PID and not clarified how the introduced Na impurities exist in the n-FE cells. In this study, we investigate Na introduction into n-FE c-Si cells by long-duration PID stress by secondary ion mass spectrometry (SIMS), scanning electron microscopy (SEM), and energy dispersive X-ray (EDX) analysis.

We used n-type wafer-based bifacial c-Si solar cells with SiN_x/Si dioxide (SiO_2) stacked passivation films cleaved into 20×20 mm^2-sized squares. We fabricated one-cell modules with the bifacial cell in the FE configuration, facing a p^+ emitter on an illumination side, through a lamination process using conventional tempered cover glass, an n-FE cell, ethylene vinyl acetate copolymer (EVA), and a polyvinyl fluoride (PVF)/polyethylene terephthalate (PET)/PVF backsheet. The details of the module fabrication process have been described elsewhere.[26] The modules then received a PID test based on the Al-plate method.[18] A negative bias of −1000 V was applied to the n-FE cell with respect to a grounded Al plate placed on the cover glass of the modules at 85 °C. Some of the n-FE PV modules underwent a recovery test in which a voltage of +1000 V was applied to the cells. We applied no intentional humidity stress, and relative humidity during the PID and recovery tests was <2%. We then measured the SIMS profiles of Na atoms in the n-FE c-Si PV cells before and after the PID tests for 12 and 480 h, which cause the second and third PID, respectively,[26] and in the cells after the recovery tests receiving the same duration of positive-bias application as the PID tests. The SIMS measurements (SIMS4550, FEI) were performed using O_2^+ as primary ions at an

acceleration voltage of 5 keV. We also observed cross-sectional SEM (FE-SEM Merlin, ZEISS) and EDX (X Flash 6130, Bruker AXS) images for the n-FE c-Si PV cells after the 480-h PID test to clarify more detailed microstructure of the degraded c-Si cells. The SEM and EDX images were captured at an electron acceleration voltage of 5 kV.

Figure 1 shows the SIMS profiles of Na atoms in n-FE c-Si cells before and after the 12-h and 480-h PID tests. The Na profiles in the n-FE cells after the recovery tests for the same duration as the PID tests were also shown. Note that the second PID can be recovered almost completely by the positive-bias application, whereas the modules showing the third PID exhibit very slight FF recovery and no V_{oc} change. The corresponding current density–voltage (J–V) characteristics for these modules were shown elsewhere.[26] One can see a broadened profile of Na atoms with a considerably high peak concentration of ~10^{19} cm^{-3} even in the n-FE cell before the PID test. This may be due to contaminants originally existing on the surface of the n-FE cell. The broadening of Na profiles probably results from the textured c-Si surface as well as a knock-on effect during the SIMS measurement. The n-FE cells receiving PID tests show SIMS profiles with much more Na concentrations than the pristine cell, which are the clear evidence of the introduction of Na into n-FE cells drifting from outside material such as cover glass. The introduction of Na into n-FE cells may cause a FF reduction for the second PID and reductions in V_{oc} and FF for the third PID. We can also confirm, from the SIMS profiles, that Na concentration in n-FE cells decrease by performing the recovery tests. This indicates the effusion of Na away from the n-FE cells by the positive-bias application, which probably leads to the recovery of FF for the n-FE cells showing the second and the third PID.[26] The results of SIMS measurements therefore seem to qualitatively reflect the PID and recovery behaviors of the n-FE c-Si PV modules.

Based on the SIMS results, one may have a picture for Na diffusing inside c-Si during the PID tests. However, the shape of the SIMS profile of Na atoms for the n-FE cell after the 480-h PID test, with a plateau near the surface, differs significantly from the others. The broadening of the SIMS profile cannot be explained by the roughness of c-Si surfaces or the knock-on effect. Furthermore, the depth of the high-density Na region is much larger than the expected diffusion length for 480 h at 85 °C, based on the extrapolated diffusion coefficient of Na in c-Si at 85 °C (on the order of 10^{-20} cm^2/s).[30] Note that a voltage of −1000 V for the PID test does not affect an electric field in c-Si and Na in c-Si can move only through diffusion. A concentration of Na detected by the SIMS measurement of ~10^{20} cm^{-3} is much larger than the solubility limit of Na in c-Si (3×10^{17} cm^{-3} at 800 °C),[31] which also quantitatively conflicts with the picture of a large number of Na diffusing into and through c-Si. We must thus observe how the introduced Na exists in the n-FE cells.

Figure 2 shows the cross-sectional SEM images of the n-FE cell receiving the 480-h PID test. The images were captured at different positions in the same n-FE cell. Dome-shaped protrusions are seen at many positions of the n-FE cell surface. The protrusions tend to be formed at the tips of c-Si pyramids. These characteristic structures are formed during the PID test. Figure 3 shows the cross-sectional SEM and EDX images of carbon (C), nitrogen (N), oxygen (O), Na, and Si atoms for one of the protrusions on the n-FE cell surface. The dome-shaped protrusion consists of Na, O, and Si, among which O may be introduced through oxidation during the air exposure of the sample after the formation of a cross-section. We thus conclude that the main contents of the protrusions are pure Na and/or Na silicide. The depth of the plateau of the Na SIMS profile near the c-Si surface for the n-FE cell after the 480-h PID test is roughly coincident with the height of the

protrusions. Since the formation of Na silicide at a temperature of as low as 85 °C is unrealistic,[32] pure Na may be more likely as the main form of the protrusions. However, we should not rule out the possibility of the existence of Na silicide because Si is also actually detected in the protrusion. One possible reason for the formation of Na-based protrusions selectively at the tips of Si pyramids is stronger electric field and resulting concentration of Na there. Note that a different result has been reported, showing no protrusions at the pyramid tips in a p-type c-Si PV cell receiving long-duration PID stress.[33] This might be due to different PID test conditions, such as humidity stress.

Another important fact found from the EDX images is that N disappears at the protrusion. This indicates that SiN_x in the vicinity of the protrusions is destroyed accompanied by the formation of the protrusions. Because SiN_x passivates the c-Si surfaces and reduces the surface recombination of carriers, the partial disappearance of SiN_x can lead to a decrease in V_{oc}. The SIMS profile of Na atoms for the cell receiving the 480-h PID test and the successive 480-h recovery test, shown in Fig. 1, displays a reduction in the density of Na and the vanishment of the plateau near the surface. This may indicate most of Na in the protrusion effuses away from the n-FE cell and the protrusion shrinks significantly. However, it is hardly possible that the destroyed SiN_x is reconstructed during the recovery test, which is consistent with the absence of V_{oc} recovery by the positive-bias application.[26] The dome-shaped protrusions may grow toward inside of the cell as well as to the outside. This may damage the p^+ emitter and the depletion region of the p–n junction of the n-FE cell and can cause a reduction in FF. Hence, we conclude that the formation of the Na-based dome-shaped protrusions is the root cause for the third PID of n-FE c-Si PV modules.

We finally discuss the second PID of the n-FE c-Si PV modules, which is

characterized by a FF reduction due to an increase in a diode ideality factor and can be recovered almost completely by applying a positive bias.[26] The SIMS profiles of Na atoms in n-FE cells after the second PID show an increase in the density of Na compared to the unstressed cell. This is, however, not a direct evidence of the invasion of Na into a depletion region of the p–n junction, since such a SIMS profile can be obtained when Na exists at SiN_x/SiO_2/c-Si interfaces, through the knock-on effect. Nevertheless, we believe that Na is the impurities introduced into the depletion region, since Na actually reaches and penetrates the p–n junction in the PID of conventional p-type c-Si PV modules.[13–16] As discussed above, the diffusion of Na in c-Si cannot quantitatively explain the introduction of Na into the depletion region locating several hundred nm away from the surface. Most possible mechanism of Na introduction into the depletion region is the formation of Na-decorated stacking faults (SFs) under the PID stress, like in the case of conventional p-type wafer-based PV modules.[13−16] Na-decorated SFs are more stable in p-type c-Si than in n-type or intrinsic ones,[34] and they can thus be, in principle, formed in the p^+ emitter. The Na-decorated SFs may reach the depletion region and act as recombination centers, resulting in an increase in a diode ideality factor and a decrease in FF. One possible reason for the absence of shunting in n-FE c-Si PV modules in the second PID may be the effect of an internal electric field existing in the depletion region, which can push back positively-charged Na ions, unlike in the case of conventional p-type wafer-based c-Si PV modules. It should be noted that the decreased FF reversely increases at the final phase of the second PID of n-FE c-Si PV modules.[26] This may be because the Na-based structures, nuclei of the protrusions, start to be formed in the final stage of the second PID, and Na in the depletion region is incorporated into the Na-based structures via the Na-decorated SFs. Based on the results of first-principle calculation for

the diffusion barriers of Na in c-Si,[35] Na can diffuse smoothly in Na-decorated SFs. Hence, the complex behaviors of the second PID of n-FE PV modules may also be related to the formation of the Na-based protrusions.

In conclusion, we found that the root cause for the third PID of n-FE PV modules is the partial destroy of SiN_x passivation films due to the formation of Na-based dome-shaped protrusions at the tips of c-Si pyramids. This is consistent with the *J–V* characteristics of the n-FE c-Si PV modules showing V_{oc} and FF reductions and almost no recovery by the positive-bias application.

The authors would like to thank Prof. Yutaka Ohno of Institute for Materials Research (IMR), Tohoku University for fruitful discussions. This work is supported by the New Energy and Industrial Technology Development Organization (NEDO).

References

1) International technology roadmap for photovoltaic (ITRPV) — 2017 Results, Technical Report (March, 2018).
2) K. Yamamoto, K. Yoshikawa, H. Uzu, and D. Adachi, Jpn. J. Appl. Phys. **57**, 08RB20 (2018).
3) K. Yoshikawa, H. Kawasaki, W. Yoshida, T. Irie, K. Konishi, K. Nakano, T. Uto, D. Adachi, M. Kanematsu, H. Uzu, and K. Yamamoto, Nat. Energy **2**, 17032 (2017).
4) K. Masuko, M. Shigematsu, T. Hashiguchi, D. Fujishima, M. Kai, N. Yoshimura, T. Yamaguchi, Y. Ichihashi, T. Mishima, N. Matsubara, T. Yamanishi, T. Takahama, M. Taguchi, E. Maruyama, and S. Okamoto, IEEE J. Photovoltaics **4**, 1433 (2014).
5) M. Taguchi, A. Yano, S. Tohoda, K. Matsuyama, Y. Nakamura, T. Nishiwaki, K. Fujita, and E. Maruyama, IEEE J. Photovoltaics **4**, 96 (2014).
6) J. Nakamura, N. Asano, T. Hieda, C. Okamoto, H. Katayama, and K. Nakamura, IEEE J. Photovoltaics **4**, 1491 (2014).
7) A. Richter, J. Benick, F. Feldmann, A. Fell, M. Hermle, and S. W. Glunz, Sol. Energy Mater. Sol. Cells **173**, 96 (2017).
8) W. Cai, S. Yuan, Y. Sheng, W. Duan, Z. Wang, Y. Chen, Y. Yang, P. P. Altermatt, P. J. Verlinden, and Z. Feng, Energy Proc. **92**, 399 (2016).
9) A. Herguth, G. Schubert, M. Kaes, and G. Hahn, Prog. Photovolt. Res. Appl. **16**, 135 (2008).
10) K. Bothe, R. Sinton, and J. Schmidt, Prog. Photovolt. Res. Appl. **13**, 287 (2005).
11) K. Bothe, R. Hezel, and J. Schmidt, Appl. Phys. Lett. **83**, 1125 (2003).
12) R. Swanson, M. Cudzinovic, D. DeCeuster, V. Desai, J. Jürgens, N. Kaminar, W. Mulligan, L. Rodrigues-Barbosa, D. Rose, D. Smith, A. Terao, and K. Wilson, Tech.

Digest 15th International Photovolt. Sci. Eng. Conf., 2005, p. 410.

13) W. Luo, Y. S. Khoo, P. Hacke, V. Naumann, D. Lausch, S. P. Harvey, J. P. Singh, J. Chai, Y. Wang, A. G. Aberle, and S. Ramakrishna, Energy Environ. Sci. **10**, 43 (2017).

14) V. Naumann, D. Lausch, A. Hähnel, J. Bauer, O. Breitenstein, A. Graff, M. Werner, S. Swatek, S. Großer, J. Bagdahn, and C. Hagendorf, Sol. Energy Mater. Sol. Cells **120**, 383 (2014).

15) V. Naumann, C. Brzuska, M. Werner, S. Großer, and C. Hagendorf, Energy Proc. **92**, 569 (2016).

16) V. Naumann, D. Lausch, A. Graff, M. Werner, S. Swatek, J. Bauer, A. Hähnel, O. Breitenstein, S. Großer, J. Bagdahn, and C. Hagendorf, Phys. Status Solidi RRL **7**, 315 (2013).

17) T. Kajisa, H. Miyauchi, K. Mizuhara, K. Hayashi, T. Tokimitsu, M. Inoue, K. Hara, and A. Masuda, Jpn. J. Appl. Phys. **53**, 092302 (2014).

18) K. Hara, H. Ichinose, T. N. Murakami, and A. Masuda, RSC Adv. **4**, 44291 (2014).

19) S. Koch, D. Nieschalk, J. Berghold, S. Wendlandt, S. Krauter, and P. Grunow, Proc. 27th European Photovoltaic Solar Energy Conf. Exhibition, p. 1985, 2012.

20) K. Mishina, A. Ogishi, K. Ueno, T. Doi, K. Hara, N. Ikeno, D. Imai, T. Saruwatari, M. Shinohara, T. Yamazaki. A. Ogura, Y. Ohshita, and A. Masuda, Jpn. J. Appl. Phys. **53**, 03CE01 (2014).

21) K. Hara, S. Jonai, and A. Masuda, Sol. Energy Mater. Sol. Cells **140**, 361 (2015).

22) S. Bae, W. Oh, K. D. Lee, S. Kim, H. Kim, N. Park, S.-I. Chan, S. Park, Y. Kang, H.-S. Lee, and D. Kim, Energy Sci. Eng. **5**, 30 (2017).

23) J. Šlamberger, M. Schwark, B. B. Van Aken, and P. Virtič, Energy **161**, 266 (2018).

24) S. Yamaguchi, A. Masuda, and K. Ohdaira, Appl. Phys. Express **9**, 112301 (2016).

25) S. Yamaguchi, K. Nakamura, A. Masuda, and K. Ohdaira, Jpn. J. Appl. Phys. **57**, 122301 (2018).

26) Y. Komatsu, S. Yamaguchi, A. Masuda, and K. Ohdaira, Microelectron. Reliab. **84**, 127 (2018).

27) S. Yamaguchi, A. Masuda, and K. Ohdaira, Sol. Energy Mater. Sol. Cells **151**, 113 (2016).

28) S. Yamaguchi, C. Yamamoto, K. Ohdaira, and A. Masuda, Prog. Photovolt. Res. Appl. **26**, 697 (2018).

29) S. Yamaguchi, C. Yamamoto, K. Ohdaira, and A. Masuda, Sol. Energy Mater. Sol. Cells **161**, 439 (2017).

30) A. V. Zastavnoi and V. M. Korol', Tech. Phys. Lett. **42**, 415 (2016).

31) J. O. McCaldin, M. J. Little, and A. E. Widmer, J. Phys. Chem. Solids **26**, 1119 (1965).

32) H. Morito, T. Yamada, T. Ikeda, and H. Yamane, J. Alloys Compounds **480**, 723 (2009).

33) M. A. Islam, T. Oshima, D. Kobayashi, H. Matsuzaki, H. Nakahama, and Y. Ishikawa, Jpn. J. Appl. Phys. **57**, 08RG14 (2018).

34) Y. Ohno, H. Morito, K. Kutsukake, I. Yonenaga, T. Yokoi, A. Nakamura, and K. Matsunaga, Appl. Phys. Express **11**, 061303 (2018).

35) B. Ziebarth, M. Mrovec, C. Elsässer, and P. Gumbsch, J. Appl. Phys. **116**, 093510 (2014).

Figure Captions

Fig. 1 SIMS profiles of Na atoms in n-FE cells before and after the 12-h and 480-h PID tests and the profiles after the recovery tests for the same duration as the PID tests.

Fig. 2 Cross-sectional SEM images of the n-FE cell after the PID test for 480 h captured at various positions.

Fig. 3 Cross-sectional SEM and EDX images of the n-FE cell after the PID test for 480 h.

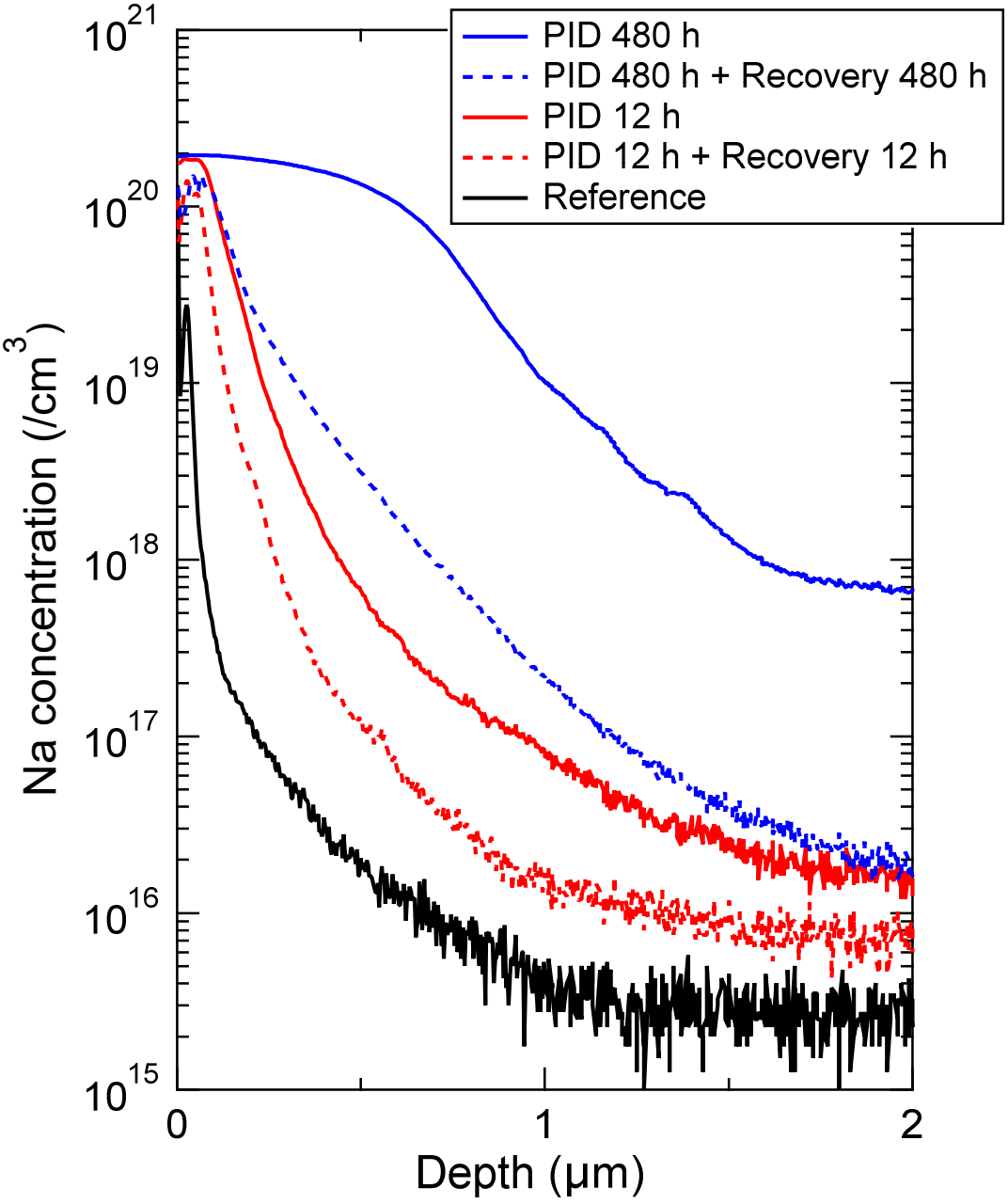

Fig. 1 K. Ohdaira et al.,

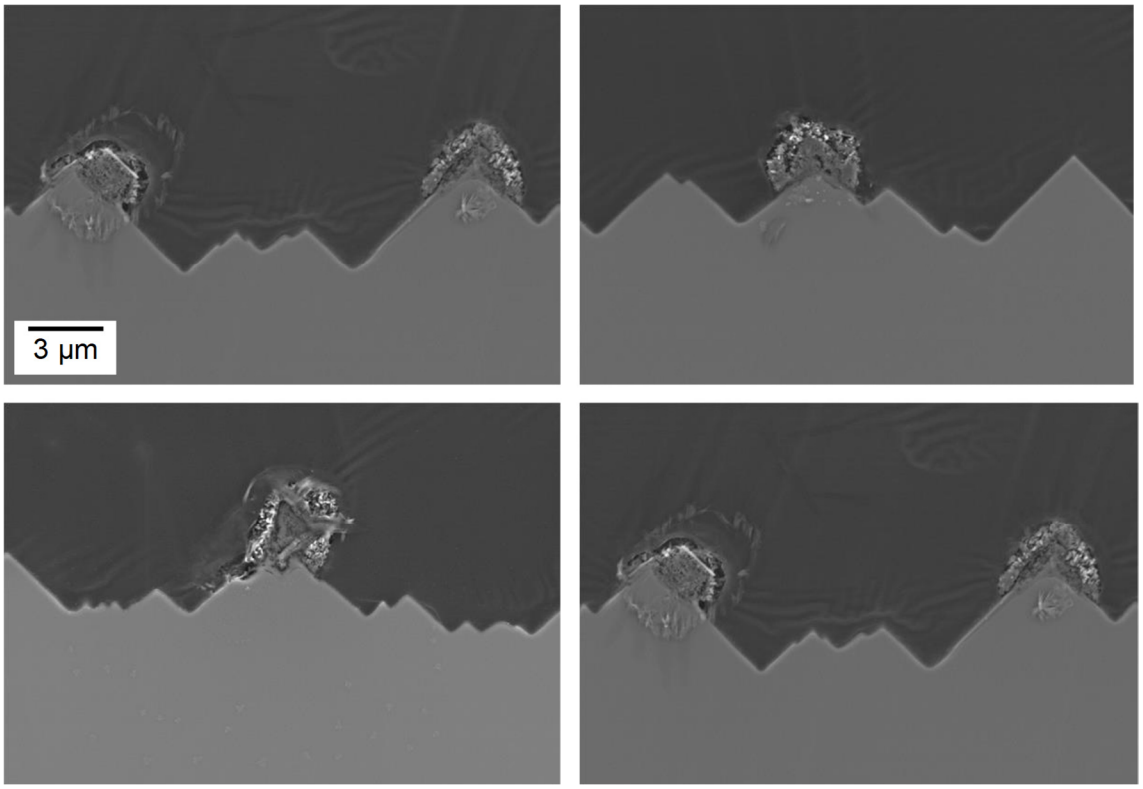

Fig. 2 K. Ohdaira et al.,

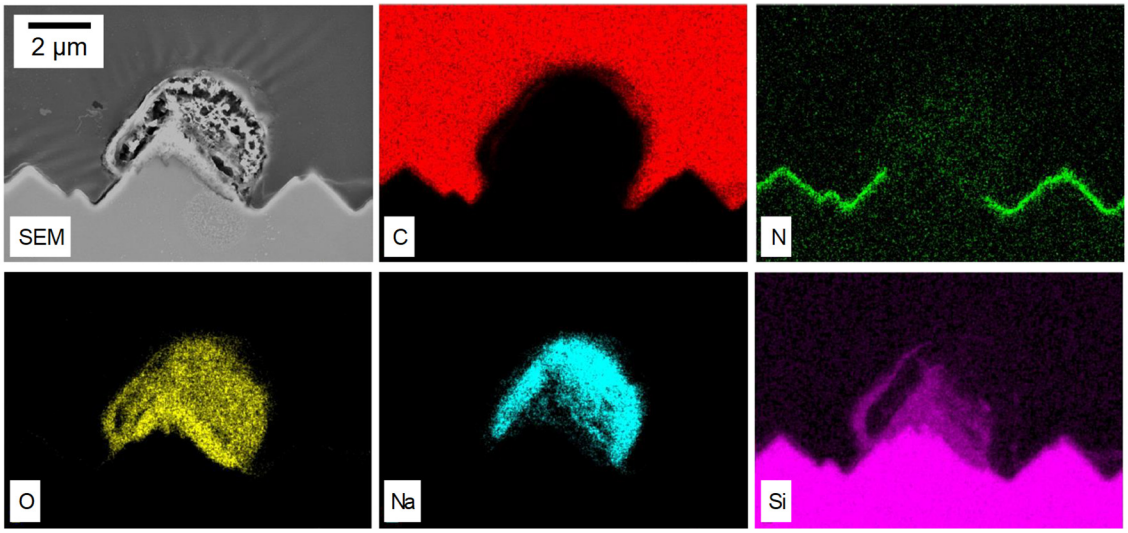

Fig. 3 K. Ohdaira et al.,